Two-photon polymerization with optimized spatial light modulator

Lóránd Kelemen
lkelemen@brc.hu

Biological Research Centre, Hungarian Academy of Sciences, Institute of Biophysics, Temesvári krt. 62, Szeged, Hungary, H-6726

Pál Ormos

Biological Research Centre, Hungarian Academy of Sciences, Institute of Biophysics, Temesvári krt. 62, Szeged, Hungary, H-6726

Gaszton Vizsnyiczai

Biological Research Centre, Hungarian Academy of Sciences, Institute of Biophysics, Temesvári krt. 62, Szeged, Hungary, H-6726

The application of diffractive optical elements can enhance the efficiency of the two- photon polymerization (TPP) process by multiplying the polymerizing beams. Spatial light modulators (SLMs) can dynamically change the light intensity pattern used for polymerization, making single shot polymerization possible. Most reflective, liquid crystal-based instruments, however, suffer from various surface aberrations. In order to enable SLMs to generate suitable polymerizing beams for TPP, these aberrations need to be corrected. Several methods were introduced earlier to compensate SLM aberrations in different applications. For the nonlinear process of TPP, we developed and specifically characterized a correction procedure. We used a simple interferometric method to determine the surface distortion of the SLM, calculated a correcting hologram and confirmed the correction with the polymerization of test structures. The corrected SLM was capable of parallel polymerization of 3D structures with a quality achievable with non-SLM beams. [DOI: 10.2971/jeos.2011.11029]

1 INTRODUCTION

The method of two-photon polymerization (TPP) to produce polymer microtools for a wide range of applications [1]-[8] has been used for more than a decade [9]-[11]. It is capable of producing structures with sub-micrometer features and can create complex 3D structures in a few straightforward steps. The method relies on focusing an ultrashort-pulsed laser beam into a layer of photoresist, where only multi-photon absorption can occur. The polymerization is confined into a well-defined volume normally bearing an ellipsoid-like shape, called the voxel [12, 13], which can have dimensions lower than the diffraction limit. TPP is capable of producing structures with feature size below 100 nm [14].

The efficiency of TPP can be improved by the multiplication of the laser beam using various diffractive optical elements such as kinoform, microlens array or spatial light modulators (SLM) [15]-[18]. Multiplication of the original laser beam by SLM has been used routinely in optical trapping experiments where it creates several, independently movable focal spots, allowing the parallel manipulation of numerous trapped objects in 3D [19]-[21]. In TPP, the control of the position of several polymerizing focal spots in 3D enables the parallel polymerization of small identical objects [16] or extended structures [17, 18]; SLM-assisted polymerization of a complex microstructure was realized even with a single, static illumination with specially tailored optical fields [22]. SLM modified beams generally suffer form a certain level of wavefront distortion due to the curvature of the reflecting surface. This is present in almost all LCoS (Liquid Crystal on Silicon) SLMs

with different severity [23]-[26], resulting in an irregular intensity distribution in the focus. In optical traps, poor focal spot characteristics lead to smaller trap stiffness and distorted force field [27, 28]. Wavefront distortion determination methods may apply wavefront sensors [29]-[31], interferometry [24] or monitor focal spot distribution [26, 28]; the correction may apply Zernike polynomials [26, 28, 31], perform the correction in domains of the SLM [32, 33] or apply a Laguerre-Gauss beam to optimize the wavefront [25]. The correction can even be performed for large area SLMs [34]. Some of these methods are intended to correct the aberrations of the entire optical pathway [32, 33], some only that of the SLM separately [24, 31, 34]. What is common is that the methods use exactly the phase shifting ability of the SLM to achieve the correction: a calculated or approximated correction hologram generates the inverse phase shift of what the surface distortion created.

During our TPP experiments, we observed strong distortions in the geometry of the resulted structures when SLM was used to create multiple polymerizing focal spots. We attributed this to the distorted focal intensity distribution that affects the regular shape of the polymerizing voxel inversely and originates from the distorted surface of the instrument. In order to polymerize microstructures with sub-micrometer features using SLM-modified beams the distortion needed to be corrected. Due to the nonlinear nature of TPP, the corrections have to be implemented and critically characterized specifically for this procedure. Our goal was to show that when a distorted-surface LCoS SLM is used in TPP its adverse effect on the

methods resolution could be eliminated by the application of a correcting hologram. We show that in order to polymerize microstructures of similar quality and reproducibility as with systems not using SLM, one must apply such a distortion correction.

We built a Michelson interferometer setup to characterize the distorting surface of the SLM, calculated a correction hologram and combined it with the holograms used for the polymerization. The system can be built easily of parts that are available in every optical lab, and did not require expensive instrumentation. The degree of the correction was characterized by polymerizing individual voxels and 3D test structures with non-SLM beam, with SLM-reflected, but uncorrected beam and with a beam reflected by the corrected SLM. We also performed SLM-assisted parallel polymerization of 3D microstructures.

2 Experimental

2.1 Two-photon polymerization setup

The light source of the TPP setup to create voxels was a femtosecond fiber laser (C-Fiber A 780, Menlo Systems GmbH, Germany, $\Delta\tau = 100$ fs, 10 nm BW, $\lambda = 780$ nm, 100 MHz repetition rate) and for the test-structures a Ti:sapphire laser (Femtorose 100, R&D Ultrafast Lasers Ltd, Hungary $\Delta\tau = 150$ fs, 6 nm BW, $\lambda = 800$ nm, 76 MHz repetition rate). The beam was focused into the sample by a 100x oil immersion objective (NA = 1.25) in two ways: either it was expanded and driven directly into the objective, or it was expanded, modified by the SLM and then directed into the objective. In the latter case, the holograms were generating either a single, corrected or uncorrected beam or several corrected beams in the 1st order. We used the acrylic-based photoresist IP-L (Nanoscribe GmbH, Germany) to polymerize individual voxels and 3D structures. 5 μL of IP-L was dropped and spread by the pipette tip over a microscope cover slip. This resist polymerizes immediately during illumination without the need of pre- or post- illumination treatment. It was developed by rinsing in 2-propanol 3 times for 5 minutes. The test structures were made of SU-8 (Microchem, USA, resin type 2007) spin-coated onto a 20 μm layer on a microscope cover slip. They were baked on a hot-plate prior to illumination for 2 minutes at 95 ^{o}C, after the illumination for 10 minutes at 95 ^{o}C to complete polymerization, developed by rinsing 3 times for 5 minutes in its developer (mr Dev-600) and finally rinsed with ethanol.

The sample was moved by a piezo-driven 3D translation system (Physik Instrumente, Germany). The individual voxels were polymerized in IP-L with a common parameter range that resulted in stable voxel formation with all types of beams (SLM-affected and non-affected as well). The goal of getting stable voxels also with the SLM-distorted beam, through which the effect can be visualized the best, required working well above the polymerization threshold of the non-distorted beam. The voxels were polymerized with laser power varied between 4 mW- 10 mW and illumination time between 10 ms and 1000 ms. At each given parameter pair a series of voxels
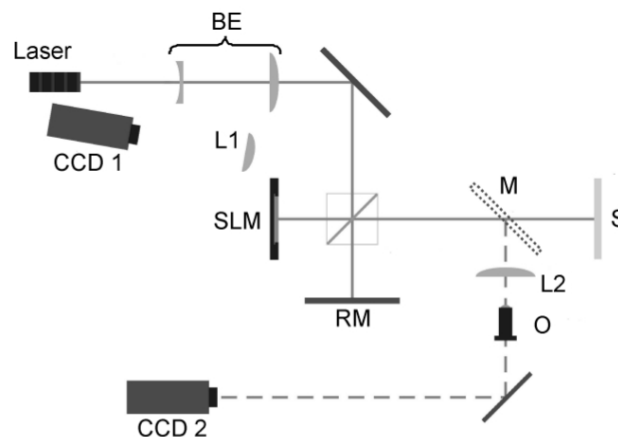

FIG. 1 Michelson interferometric setup for the determination of the surface curvature of the SLM used for TPP. BE: beam expander; RM: reference mirror; CCD1 and CCD2 are used to digitize the interferogram or the focused images, respectively; S: screen; L1 and L2 are 125 mm and 100 mm lenses, respectively; O: 20x microscope objective; M: optional mirror.

were polymerized by shifting the z positions of the consecutive voxels in 250 nm steps thereby truncating them at various heights. 2-10 mW laser power and 1-12 μm/s scanning speed was used to polymerize the SU-8 test structures. The geometric features of the resulted structures were measured on scanning electron micrographs using Matlab algorithms. In the TPP experiments a reflective LCoS display-based SLM was used with 1024x768 pixels resolution (LC-R 2500, Holoeye Photonics AG, Germany). Prior to the experiments the phase modulation of the display as the function of the grayness level of the hologram was linearized [35]. We determined that the device is capable of more than 2π phase shift in the 400- 700 nm wavelength range but at the polymerizing 800 nm it is only 1.6π.

2.2 SLM surface distortion measurement setup

The surface curvature of the SLM display was determined by a home-built Michelson- interferometric setup (Fig. 1). The expanded (BE) beam of a 532 nm CW solid-state laser was used as light source primarily because of its suitable coherence length as opposed to the 35 μm coherence length of the polymerizing beam. In the arrangement, the interferogram observed on a screen (S) was projected (lens L1) onto a monochrome CCD camera (CCD1), and recorded as a video stream. Alternatively, the reference mirror- (RM) or the SLM-reflected beam was focused (L2) and projected (20x microscope objective O) onto a second CCD camera (CCD2) to inspect focal plane intensity distribution.

The SLM surface curvature was calculated from the observed interferogram by a home- developed program (Matlab, The Mathworks Inc., Natick, MA, U.S.A.). Since the observed interferogram is not uniquely determined by the surface distortions, i.e. various surface distortions could generate the observed interferogram, we had to apply one assumption for the hologram calculations: the SLM display is a simple concave surface with one minimum approximately in its center. This is supported by the literature [26], and also by discus-
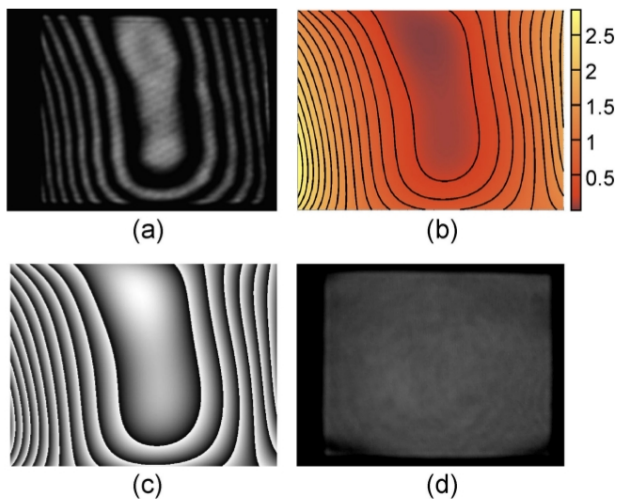
FIG. 2 (a) Interferogram obtained with $\lambda = 532$nm, extended to the aperture of the SLM. (b) Representation of the calculated SLM surface (contour lines represent equal height values, height scale is in micrometers). (c) The calculated correcting hologram for 532 nm and (d) the measured interferogram with the correcting hologram displayed on the SLM. The supplementary media file shows the effect of correction for 532 nm with switching the correcting hologram OFF and ON.
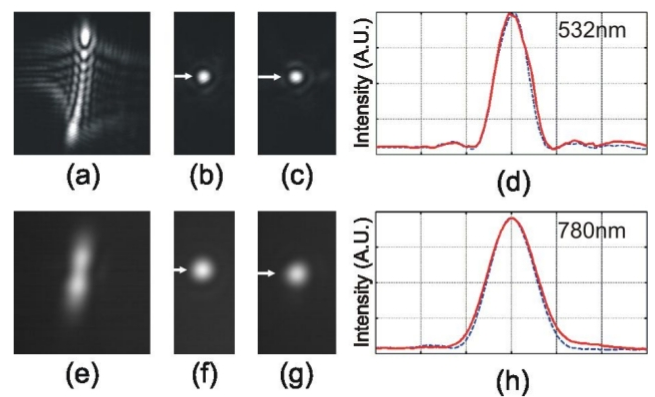

FIG. 3 Intensity distributions of focused 532 nm laser beam in the cases of (a) NonC-SLM, (b) No-SLM and (c) C-SLM. (d) Normalized intensity profiles of (b) (dashed) and (c) (continuous), respectively, measured in the direction of the arrows. Intensity distributions of focused 780 nm laser beam in the cases of (e) NonC-SLM, (f) No-SLM and (g) C-SLM. (h) Normalized intensity profiles of (f) (dashed) and (g) (continuous), respectively, measured in the direction of the arrows.

2.4 Calculation of the correcting hologram

The known surface allows the calculation of a correcting hologram for any given wavelength (for $\lambda = 532$ nm see (Fig. 2(c)). This can be carried out simply by calculating the $\mathrm{mod}(\pi/2)$ of the height matrix representing the surface and then transforming each matrix element linearly into an 8-bit grayscale image.

3 Results

3.1 Testing the correction hologram

The calculated surface indicates that there is 2.86 μm peak-to-valley difference over the display of the SLM (Fig. 2(b)). The surface is mostly bending around the vertical axis, similarly to a cylindrical mirror. Interestingly, the middle section of the display (a 250x250 pixels, or 5x5 mm area) has less than 200 nm P-V distortion, enabling its use without correction. However, to take advantage of the full resolution of the SLM, one must illuminate its entire surface.

From now on, we refer to the original beam not reflected from the SLM as **No-SLM**, to the beam reflected from the uncorrected SLM as **NonC-SLM**, and to the beam reflected from the corrected SLM as **C-SLM**. The SLM-reflected beams were always deviated to the 1st order from the unaffected 0th order by a blazed grating hologram. In the case of NonC-SLM, the grating hologram was used alone, in the C-SLM case it was added to the correcting hologram.

The calculated correcting hologram was tested by recording the C-SLM beams interferogram with the reference beam and also by recording its intensity distribution in the focal plane. The interferogram recorded with the 532 nm C-SLM beam is shown in Fig. 2(d). The intensity depicts the beam's residual phase front error. The intensity minima, seen on Fig. 2(a), are completely eliminated from the central region, and the residual peak-to-valley distortion regarding the entire surface is less than $\lambda/4$.

sions with the manufacturer. The calculated correcting phase shift pattern for 780 nm was tested by comparing the intensity distributions of the original, the SLM-distorted and the corrected beams and by TPP experiments.

2.3 Measurement of the SLM surface curvature

We calculated the SLM curvature from the positions of the observed intensity maxima and minima of the interferogram. In order to determine the positions of these maxima and minima we applied various image-processing algorithms of Matlab on the recorded interferogram. From our initial assumption it follows that the neighboring intensity maxima and minima lines refer to such contour levels on the SLM that are of the same height relative to a lowest point. These levels reflect the incoming light with $\lambda/4$ path difference (in our case 133 nm). Therefore we approximated the SLM surface using these lines as reference levels.

First, the static interferogram was centered on the screen resulting in a single, averaged quasi- symmetric grayscale image (Fig. 2(a)). On this image, the positions of the interferogram maxima and minima lines were determined using image processing routines such as contrast enhancement, level-filtering, erosion, which resulted in a 1-bit image. These lines were then assigned to pixel positions on the surface of the SLM. The assignment involved the precise scaling and centering of the 1-bit image on the device with the assist of a rectangular mesh pattern displayed on it. We assigned 0nm height to the centermost line and such height values to the rest of the lines, which were incrementally increasing in the outward direction in 133 nm steps. The surface finally was re-created by fitting fourth-order polynoms to the height values (Fig. 2(b)).

The effect of the correction on the focal plane intensity distribution, a crucial parameter in TPP, can be seen on Fig. 3. When focusing the NonC-SLM beam either at 532 nm (Fig. 3(a)) or at 780 nm (Fig. 3(e)), two perpendicular focal lines are observed similarly to an astigmatic system. This is in accordance with the calculated surface, which is bent mostly around the vertical axis. The distortion can be eliminated completely at 532 nm (Fig. 3(c)), and almost completely at 780 nm (Fig. 3(g)) by the application of the correcting hologram. The C-SLM 532 nm beam is of circular shape, its FWHM is only about 6 % larger than that of the reference No-SLM beam and has somewhat larger side lobes. The correcting hologram also resulted in a circular focal spot in the case of the 780 nm beam (Fig. 3(g)), however the improvement is of smaller degree: the shape is slightly not circular, also has larger side-lobes and the FWHM in the indicated direction is about 9 % larger than that of the No-SLM beam (Fig. 3(f)). We believe that this is due to the only 1.6 π phase shift what the SLM is capable of around 780nm.

3.2 Application of the corrected beam for TPP

The goal of the SLM correction was to optimize beam quality for TPP when SLM is used. In order to quantify the effect of the correction, individual voxels and 3D test structures were polymerized using the three different beams: No-SLM, NonC-SLM, and C-SLM. In both of the last two cases a single beam deflected into the 1st order was used. The voxels are the building blocks of the TPP structures; therefore, the effect of the distorted beam on a 3D TPP structure can be effectively studied through the distortion of their shape. The simplest elements of any 3D TPP structure that already involves translation of the focal spot are straight lines so we also examined the distorting effect on polymerized lines constituting the test structures. In the described parameter range we studied i) how the polymerization threshold, ii) how the shape of the polymerizing voxel, and iii) how the eventual dimensions of the voxels and scanned lines depend on the three types of beams.

Using the NonC-SLM beam, no IP-L voxel could be made at the lowest 4 mW power even using 1000 ms illumination time, however, with the No-SLM and C-SLM beams at 4 mW with 20 ms it was still possible. For the SU-8 test structures polymerized by the NonC-SLM beam, intact structures were found only at and above 6 mW, at this power only below 4 μm/s scan speed; with No-SLM and C-SLM beams, they were intact even at 2 mW power (at this power only below 2 μm/s scan speed).

Fig. 4(a) shows that the voxels made with the No-SLM beam has indeed a regular ellipsoid-like shape with a circular cross section. This results straight lines of equal width along the x and y axis and rods along the z axis on the test structures (Fig. 4(e)). The effect of aberration of the NonC-SLM beam is present in the entire parameter range we studied, with higher visibility at higher laser power. The polymerized voxels consist of two perpendicular planes inheriting the directions of the focal lines of the astigmatic focal spot. The shift of the consecutive focal spots in the z direction allows a better visualization of the shape. On Fig. 4(c) the emerging of such a voxel can be followed in the direction of the arrows: first,
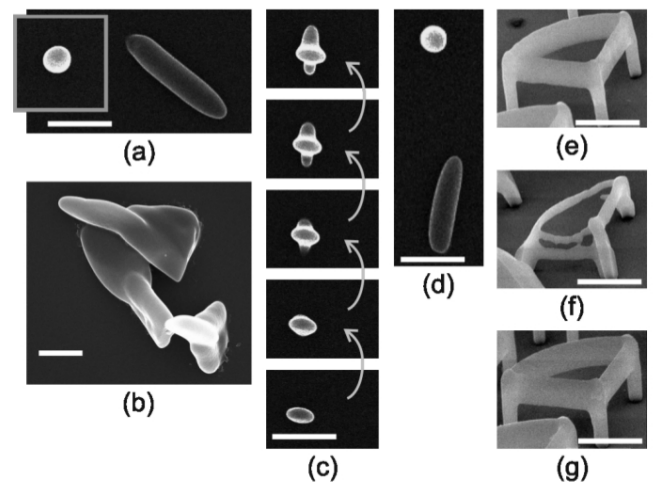

FIG. 4 Electron-micrographs of IP-L individual voxels ((a)-(d)) and SU-8 test structures ((e)-(g)) polymerized with No-SLM ((a), (e)), NonC-SLm ((b), (c), (f)) and C-SLM ((d), (g)) beams. The voxels were polymerized with 6 mW laser power and 20 ms illumination time ((a), (c), (d)) and 10 mW and 1000 ms illumination time (b); the test structures with 6 mW laser power and 4 μm/s scan speed. Scale bar for voxels: 1 μm, for test structures: 5 μm.
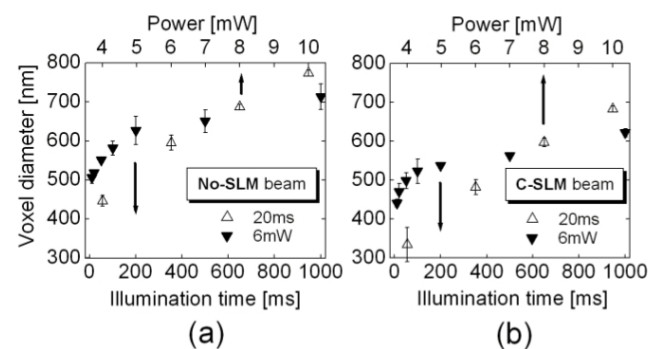

FIG. 5 Diameter of the polymerized voxels made by the (a) No-SLM and (b) C-SLM beams. Closed triangles: illumination time dependence at 6 mW laser power; open triangles: laser power dependence at 20 ms illumination time.

one planar half of the vortex polymerized by one of the focal lines appears, then gradually the perpendicular one producing an eventual cross-shaped cross section. At 10 mW laser power, 1000 ms illumination time even the structured internal intensity distribution of the astigmatic polymerizing beam can be seen (Fig. 4(b)). Here, 3 such voxels are shown, displaying the two perpendicular planar voxel halves at various angles. The test structures are completely distorted and often collapse when polymerized with this beam (Fig. 4(f)). The restoring effect of the correcting hologram applied on the SLM is, however, evident (Fig. 4(d)): the voxel again has a circular cross section with an ellipsoid- like shape. On the test structures, the straight lines (Fig. 4(g)) again obey the same geometry as those made with the No-SLM beams.

We compared the diameter of the voxels made by the No-SLM (Fig. 5(a)) and the C-SLM (Fig. 5(b)) beams. The dependence on the illumination time at 6 mW laser power and that on the laser power at 20 ms illumination time are presented for both cases. Although these parameter ranges resulted in stable voxels also for the NonC-SLM, their cross-shaped voxels did not

have a well- defined width, therefore could not be compared quantitatively.

As a general observation, the diameter of the polymerized voxels follow the same trend both in the case of the No-SLM and in the C-SLM case: at 6mW power both are breaking down at about 100 ms ilumination time, and using 20 ms illumination time both are almost linear in the 4 mW-10 mW power range. We attribute the difference between the diameters measured at identical parameters to the not fully recovered intensity distribution of the corrected beam. We considered the dependency of the width in the applied power regime to be linear: for the No- SLM beam 53 nm/mW slope is achieved, for the C-SLM beam it is 58 nm/mW. The run of the curves anticipate that the diameter values could be further reduced [9, 36], especially with reducing the applied power. However, in that parameter range the NonC-SLM beam does not result in any voxel, so the comparison of their shape is not possible. The thickness of the straight lines of the SU-8 test structures also display similar linear dependence with laser power at the applied scan speeds for the No-SLM and C-SLM beams (not shown).

The fact, that the geometry of the voxels made by the C-SLM beam behaves qualitatively the same way as the No-SLM beam suggests that it is just as possible to produce reproducible microstructures with the corrected beam as with the original one. On the contrary, the double, perpendicular focal planes polymerized with the NonC-SLM beam makes it impossible. Considering the use of λ = 780 nm beam, which is out of the SLMs design range, we believe that this degree of correction enables the device to produce two-photon polymerized microstructures with greater efficiency.

In order to demonstrate the increase of efficiency we performed parallel polymerization of the test structures from SU-8 by splitting the original beam to six beams and of the more complicated 3D logo of our institute from IP-L with 4 beams. For the first, the hologram resulted in a 2-by-3 arrangement of the polymerizing focal spots, placed 12 μm from each other (Fig 6.(a)), for the second one a 2-by-2 arrangement with dx = 15 μm and dy = 20 μm distances. The six beams feature a uniformity of U = 0.956 where U = 1-(Pmax-Pmin)/(Pmax+Pmin) where Pmax and Pmin are the integrated maximal and minimal focal spot intensity values in the 6 beams, respectively. The paralelly polymerized test structures (Fig. 6(b)) possess the same geometric characteristics as the structure made by only one C-SLM beam (Fig. 4(g)) and are practically indistinguishable from each other. Also, the parallel polymerization of the logos resulted in identical 3D structures. We conclude that the C-SLM beams are not only capable of producing TPP microstructures of similar quality as No-SLM beams, but using SLM greatly enhances the efficiency of the procedure being able to make multiple identical structures.

4 Conclusion

We optimized the use of a spatial light modulator in a two-photon polymerization setup by calculating and correcting its surface curvature. First, we determined the shape of its dis-
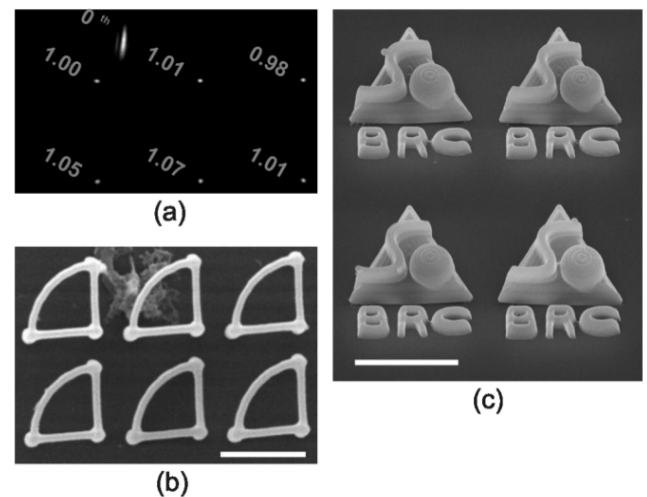

FIG. 6 (a) Focal spot arrangement of 6 polymerizing C-SLM beams generated in the first order and the non-corrected zero order beam in the sample plane. The normalized numbers on the left of each spot represent the relative intensity of that beam. (b) Electron micrographs of 6 SU-8 test structures polymerized in parallel mode by the 6 beams shown in (a) (6 mW power in each beam, 4 μm/s scan speed). (c) Electron micrographs of the parallel-polymerized logo of our institute made of IP-L by 4 C-SLM beams (6.3 mW power in each beam, various scan speeds; imaged with 30 degrees tilt). Scale bars are 10μm.

torted surface by a Michelson interferometric setup, and then we calculated a correction hologram for the polymerizing 780 nm wavelength. The tests showed that the about 5 λ phase front distortion of the SLM-reflected beam could be reduced to below $\lambda/4$ in the region of the SLM used for TPP. The intensity distribution of the focused beam could be restored with the deviation of the width less than 10 % from the reference beam at 780 nm and with a beam profile slightly off-Gaussian, compatible with the result of most of the wavefront-compensation methods. Most importantly, as opposed to the non-corrected SLM, the shapes of the voxels can be restored completely and highly regular structures can be produced. The application of the correcting hologram demonstrates the restoring power of the applied surface aberration correction method, and enables the SLM to increase the efficiency of TPP. The improvement of the SLM-based TPP setup is an ongoing work applying methods to correct not only the distortion of the SLM itself but that of the entire optical path.

5 Acknowledgement

References

[1] B. H. Cumpston, S. P. Ananthavel, S. Barlow, D. L. Dyer, J. E. Ehrlich, L. L. Erskine, A. A. Heikal, S. M. Kuebler, I.-Y. S. Lee, D. McCord-

Maughon, J. Qin, H. Röckel, M. Rumi, X.-L. Wu, S. R. Marder, and J. W. Perry, "Two-photon polymerization initiators for three dimensional optical data storage and microfabrication", Nature **398**, (6722), 51- 54 (1999).

[2] S. Kawata, H. B. Sun, T. Tanaka, and K. Takada, "Finer features for functional microdevices - Micromachines can be created with higher resolution using two-photon absorption", Nature **412**, (6848) 697-698 (2001).

[3] P. Galajda and P. Ormos, "Complex micromachines produced and driven by light", Appl. Phys. Lett. **78**, 249-151 (2001).

[4] R. Guo, S. Z. Xiao, X. M. Zhai, J. W. Li, A. D. Xia, and W. H. Huang, "Micro lens fabrication by means of femtosecond two photon photopolymerization", Opt. Express **14**, 810-816 (2006).

[5] S. Maruo, and H. Inoue, "Optically driven micropump produced by three-dimensional two-photon microfabrication", Appl. Phys. Lett. **89**, 144101 (2006).

[6] L. Kelemen, S. Valkai, and P. Ormos, "Integrated optical motor", Appl. Optics **45**, 2777- 2780 (2006).

[7] G. Knöner, S. Parkin, and T. A. Nieminen, V. L. Y. Loke, N. R. Heckenberg, H. Rubinsztein-Dunlop, "Integrated optomechanical microelements", Opt. Express **15**, 5521-5530 (2007).

[8] S. Maruo, A. Takaura, and Y. Saito, "Optically driven micropump with a twin spiral microrotor", Opt. Express **17**, 18525-18532 (2009).

[9] K.-S. Lee, R. H. Kim, D.-Y. Yang, S. H. Park, "Advances in 3D nano/microfabrication using two-photon initiated polymerization", Prog. Polym. Sci. **33**, 631-681, (2008).

[10] S-H. Park, D-Y. Yang, and K-S. Lee, "Two-photon stereolithography for realizing ultraprecise three-dimensional nano/microdevices", Laser Photonics Rev. **3**, 1-11 (2009).

[11] S. D. Gittard and R. J. Narayan, "Laser direct writing of micro- and nano-scale medical devices", Expert Rev. Med. Devic. **7**, 343-356 (2010).

[12] H.-B. Sun, T. Tanaka, and S. Kawata, "Three-dimensional focal spots related to two- photon excitation", Appl. Phys. Lett. **80**, 3673-3675 (2002).

[13] T. Tanaka, H. Sun, and S. Kawata, "Rapid Sub-Diffraction-Limit Laser micro/ nanoprocessing in a Threshold Material System", Appl. Phys. Lett. **80**, 312-314 (2002).

[14] W. Haske, V. W. Chen, J. M. Hales, W. T. Dong, S. Barlow, S. R. Marder, and J. W. Perry, "65 nm feature sizes using visible wavelength 3-D multiphoton lithography", Opt. Express **15**, 3426-3436 (2007).

[15] F. Formanek, N. Takeyasu, T. Tanaka, K. Chiyoda, A. Ishikawa, and S. Kawata, "Three-dimensional fabrication of metallic nanostructures over large areas by two- photon polymerization", Opt. Express **14**, 800-809 (2006).

[16] L. Kelemen, S. Valkai, and P. Ormos, "Parallel photopolymerisation with complex light patterns generated by diffractive optical elements", Opt. Express **15**, 14488-14497 (2007).

[17] H. Takahashi, S. Hasegawa, A. Takita, and Y. Hayasaki, "Sparse-exposure technique in holographic two-photon polymerization", Opt. Express **16**, 16592-16599 (2008).

[18] R. J. Winfield, B. Bhuian, S. O' Brien, G.M. Crean, "Fabrication of grating structures by simultaneous multi-spot fs laser writing", Appl. Surf. Sci. **253**, 8086-8090, (2007).

[19] D. G. Grier, "A revolution in optical manipulation", Nature **424**, (6950), 810-816 (2003).

[20] J. Leach, G. Sinclair, P. Jordan, J. Courtial, M. Padgett, J. Cooper, and Zs. Laczik, "3D manipulation of particles into crystal structures using holographic optical tweezers", Opt. Express **12**, 220-226 (2004).

[21] A. Jesacher, C. Maurer, A. Schwaighofer, S. Bernet, and M. Ritsch-Marte, "Full phase and amplitude control of holographic optical tweezers with high efficiency", Opt. Express **16**, 4479-4486 (2008).

[22] G. Bautista, M. J. Romero, G. Tapang, and V. R. Daria, "Parallel two-photon photopolymerization of microgear patterns", Opt. Commun. **282**, 3746-3750 (2009).

[23] K. Seunarine, D. W. Calton, I. Underwood, J. T. M. Stevenson, A. M. Gundlach, and M. Begbie, "Techniques to improve the flatness of reflective micro-optical arrays", Sensor Actuator **78**, 18-27 (1999).

[24] T. Inoue, H. Tanaka, N. Fukuchi, M. Takumi, N. Matsumoto, T. Hara, N. Yoshida, Y. Igasaki, and Y. Kobayashi, "LCOS spatial light modulator controlled by 12-bit signals for optical phase-only modulation", Proc. SPIE **6487**, 64870Y (2007).

[25] A. Jesacher, A. Schwaighofer, S. Fürhapter, C. Maurer, S. Bernet, and M. Ritsch- Marte, "Wavefront correction of spatial light modulators using an optical vortex image", Opt. Express **15**, 5801-5808 (2007).

[26] E. Martín-Badosa, M. Montes-Usategui, A. Carnicer, J. Andilla, E. Pleguezuelos, and I. Juvells, "Design strategies for optimizing holographic optical tweezers set-ups", J. Opt. A - Pure Appl. Op. **9**, S267-S277, (2007).

[27] Y. Roichman, A. Waldron, E. Gardel, and D. G. Grier, "Optical traps with geometric aberrations", Appl. Opt. **45**, 3425-3429 (2006).

[28] K. D. Wulff, D. G. Cole, R. L. Clark, R. DiLeonardo, J. Leach, J. Cooper, G. Gibson, and M. J. Padgett, "Aberration correction in holographic optical tweezers", Opt. Express **14**, 4169-4174 (2006).

[29] C. Li, M. Xia, Q. Mu, B. Jiang,, L.i Xuan, and Z. Cao, "High-precision open-loop adaptive optics system based on LC-SLM", Opt. Express **17**, 10774-10781 (2009).

[30] C. López-Quesada, J. Andilla, and E. Martín-Badosa, "Correction of aberration in holographic optical tweezers using a Shack-Hartmann sensor", Appl. Opt. **48**, 1084- 1090 (2009).

[31] J. Garcia-Marquez, J.E.A. Landrave, N. Alcala-Ochoa, C. Perez-Santos, "Recursive wavefront aberration correction method for LCoS spatial light modulators", Opt. Laser Eng. **49**, 743-748 (2011).

[32] R. W. Bowman, A. J. Wright and M. J. Padgett, "An SLM-based Shack-Hartmann wavefront sensor for aberration correction in optical tweezers", J. Opt. **12**, 124004 (2010).

[33] T. Cizmar, M. Mazilu, K. Dholakia, "In situ wavefront correction and its application to micromanipulation", Nat. Photonics **4**, 388-394 (2010).

[34] L. Hu, L. Xuan, Y. Liu, Z. Cao, D. Li, and Q. Mu, "Phase-only liquid crystal spatial light modulator for wavefront correction with high precision", Opt. Express **12**, 6403- 6409 (2004).

[35] http://holoeye.com/download_daten/PhaseCam_Manual.pdf

[36] H. B. Sun, K. Takada, M. S. Kim, K.-S. Lee, and S. Kawata, "Scaling laws of voxels in two-photon photopolymerization nanofabrication", Appl. Phys. Lett. **83**, 1104-1106 (2003).